remote sensing

MDPI

Article

Dry Season Evapotranspiration Dynamics over Human-Impacted Landscapes in the Southern Amazon Using the Landsat-Based METRIC Model

Kul Khand [1], Izaya Numata [2,*], Jeppe Kjaersgaard [3] and George L. Vourlitis [4]

[1] Biosystems and Agricultural Engineering Department, Oklahoma State University, Stillwater, OK 74078, USA; kul.khand@okstate.edu
[2] Geospatial Sciences Center of Excellence, South Dakota State University, Brookings, SD 57007, USA
[3] South Dakota Water Resources Institute, South Dakota State University, Brookings, SD 57007, USA; jeppe.kjaersgaard@sdstate.edu
[4] Department of Biological Sciences, California State University San Marcos, San Marcos, CA 92096, USA; georgev@csusm.edu
* Correspondence: izaya.numata@sdstate.edu; Tel.: +1-605-688-5227

Academic Editors: Zhaoliang Li, Clement Atzberger and Prasad S. Thenkabail
Received: 24 May 2017; Accepted: 5 July 2017; Published: 9 July 2017

Abstract: Although seasonal and temporal variations in evapotranspiration (ET) in Amazonia have been studied based upon flux-tower data and coarse resolution satellite-based models, ET dynamics over human-impacted landscapes are highly uncertain in this region. In this study, we estimate ET rates from critical land cover types over highly fragmented landscapes in the southern Amazon and characterize the ET dynamics during the dry season using the METRIC (Mapping Evapotranspiration at high Resolution with Internalized Calibration) model. METRIC, a Landsat-based ET model, that generates spatially continuous ET estimates at a 30 m spatial resolution widely used for agricultural applications, was adapted to the southern Amazon by using the NDVI indexed reference ET fraction (ET_rF) approach. Compared to flux tower-based ET rates, this approach showed an improved performance on the forest ET estimation over the standard METRIC approach, with $R^2 = 0.73$ from $R^2 = 0.70$ and RMSE reduced from 0.77 mm/day to 0.35 mm/day. We used this approach integrated into the METRIC procedure to estimate ET rates from primary, regenerated, and degraded forests and pasture in Acre, Rondônia, and Mato Grosso, all located in the southern Amazon, during the dry season in 2009. The lowest ET rates occurred in Mato Grosso, the driest region. Acre and Rondônia, both located in the southwestern Amazon, had similar ET rates for all land cover types. Dry season ET rates between primary forest and regenerated forest were similar ($p > 0.05$) in all sites, ranging between 2.5 and 3.4 mm/day for both forest cover types in the three sites. ET rates from degraded forest in Mato Grosso were significantly lower ($p < 0.05$) compared to the other forest cover types, with a value of 2.03 mm/day on average. Pasture showed the lowest ET rates during the dry season at all study sites, with the dry season average ET varying from 1.7 mm/day in Mato Grosso to 2.8 mm/day in Acre.

Keywords: evapotranspiration; METRIC; Amazon

1. Introduction

The Amazon Basin holds nearly half of all remaining tropical rainforest [1,2], playing an important role in regional hydrological cycles. Tropical forests exchange large amounts of water through evapotranspiration (ET) [3]. Nearly half of all water released to the atmosphere by ET is recycled as precipitation in the Amazon basin [4]. However, spatial and seasonal ET variability is substantial across Amazonia. For example, forest ET in the wet equatorial Amazon is maintained or higher in the dry

season than the wet season due to higher net radiation and a deep root system [5,6]. In the south, under the longer dry season and more severe water stress conditions, more dynamic and variable ET patterns are found, e.g., higher in the dry season than the wet season and vice-versa, as a function of several factors including vegetation type, depth to the water table, and surface conductance [7,8]. Although forest ET plays an important role in moisture recycling during the dry season and is essential for withstanding a potentially drier climate in the Amazon [9], the Amazon forest has been heavily altered by anthropogenic disturbances including deforestation, selective logging and fragmentation, and climate impacts such as drought and resultant wild fire [10–13]. Regional variations and seasonal trends of ET across a biome gradient from tropical forest to savanna in the Amazon have been studied using flux tower data [5,6,13–16], and ET dynamics from highly fragmented landscapes with a complex combination of different land cover types (e.g., pasture/crop areas, secondary forests, and degraded forests) are not well known. In order to investigate how ET varies across fragmented landscapes, spatially continuous and high spatial resolution ET data are necessary.

Satellite-based models provide spatially continuous ET information at landscape to regional and global scales [17–20]. Currently, ET products derived from remote sensing for Amazonia are coarse in spatial resolution ($\geq$1 km) and are obtained from platforms such as MODIS [21,22]. While these ET estimates are very valuable and useful for, e.g., understanding spatially integrated regional ET patterns, they are not able to capture finer scale variations. Other remote sensing-based ET models utilize satellite images at a higher resolution. Within these models, METRIC (Mapping Evapotranspiration at high Resolution with Internalized Calibration) utilizes Landsat imagery to compute actual ET as a residual of the surface energy balance. The information from the Landsat images is combined with ground-based meteorological inputs to produce high resolution (30 m) ET maps [23]. While primarily used for agriculture, METRIC has also been successfully applied over different land use and land cover types including forest [24–28].

In the Amazon, [28] evaluated METRIC to estimate ET rates from tropical forests. While METRIC derived ET rates were well correlated with ET rates from a flux tower, their analysis also highlights a challenge with the calibration of this model for the dry season condition in the Amazon. METRIC calibrates the sensible heat (H) component of the surface energy balance by determining two extreme ET conditions [24]. These extreme ET conditions, i.e., the lowest and highest ET, are represented through the selection of anchor pixels (hot and cold pixels) within the satellite image. The hot pixel is selected from the bare soil surface where ET is assumed to be near zero, whereas the cold pixel represents the maximum ET and is usually selected from actively and vigorously growing agricultural crops fully covering the ground. However, the selection of the cold anchor pixel used in METRIC calibration is challenging during the dry season in the Amazon due to the difficulty of identifying ideal, fully vegetated, and wet conditions for a cold pixel extraction [24]. While the Landsat-based METRIC model has the potential to provide high spatial ET data required for assessing the effects of land use on hydrological cycles in highly fragmented landscapes, this model needs to be better adapted to the dry season conditions in the Amazon region.

This study addressed two main objectives: (1) adaptation of METRIC to the Amazon region; and (2) characterization of fine spatial scale, dry season ET dynamics from different land cover types in fragmented landscapes in the southern Amazon. We apply METRIC to three geographic locations, namely, Acre, Rondônia, and Mato Grosso (Figure 1). These sites are located in a region called the "Arc of Deforestation", where forests are highly fragmented and are subject to other disturbances such as forest fire [29–31]. This region undergoes a three to five month long dry season each year and presents substantial seasonal variations in ET [7,8,13]. Thus, the high spatial data provided from Landsat is likely to be preferable to other satellite-based data for estimating ET in this region.

This study consists of two parts. First, we compared METRIC-based ET estimates with flux tower ET estimates from two study sites (Rondônia and Mato Grosso). For this comparison, we tested an NDVI-based approach to adapt the METRIC model to Amazonian tropical forest conditions as opposed to the standard METRIC approach designed for croplands. After evaluating the performances

of these approaches, we applied the improved METRIC approach in three study sites in the southern Amazon to characterize the ET dynamics of primary, regenerated, and degraded forests and pastures in the 2009 dry season.

2. Study Sites and Data

Our study focuses on the southern Amazon Basin, a seasonally dry region where intensive land cover and land use change has occurred in the past decades. Three Landsat path/row scenes were selected from three states of the Brazilian Amazon, i.e., Acre (path/row = 1/67), Rondônia (231/67), and Mato Grosso (226/68) (Figure 1, Table 1). These states exhibit a pronounced dry season but with different degrees of seasonality (Figure 2). Mato Grosso presents the lowest precipitation level with the longest dry season of four to five months, whereas Rondônia and Acre have a dry season that lasts three to four months. These three sites contain seasonally dry semi-deciduous forests. The study sites present a period of water deficit for four to seven months, when precipitation is lower than ET [7].

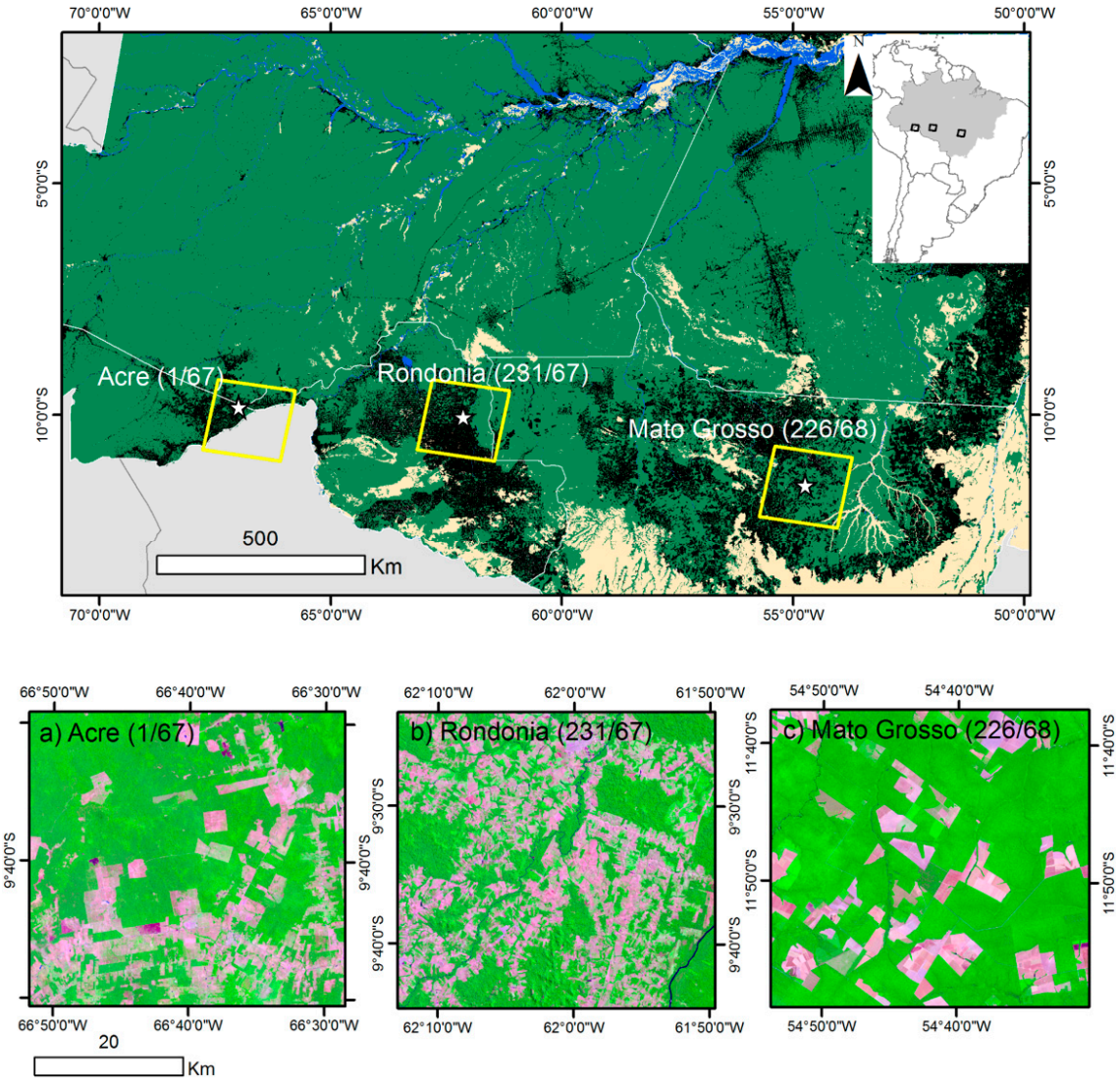

Figure 1. The three study sites within the State of (**a**) Acre (1/67); (**b**) Rondônia (231/67); and (**c**) Mato Grosso (226/68) in the southern Brazilian Amazon (Landsat false color composite images with bands 5, 4, and 3 in RGB).

Table 1. Summary of study site and weather station/flux tower information.

Landsat Path/Row (State)	Weather Station/Flux Tower (Location)	Vegetation Type at (Height)	Study Year
1/67 (Acre)	INMET-A104 (9.957 S, 98.165 W)	pasture (0.5 m)	2008–2010
231/67 (Rondônia)	FNS (10.762 S, 62.357 W)	pasture (0.5 m)	2000–2002
	INMET-A940 (9.949 S, 62.962 W)	pasture (0.5 m)	2009
	Jaru (10.078 S, 61.933 W)	forest (30 m)	2000–2002
226/68 (Mato Grosso)	INMET-A917 (11.982 S, 55.566 W)	pasture (0.5 m)	2007–2008
	INMET-A904 (12.555 S, 55.723 W)	pasture (0.5 m)	2009
	Sinop (11.414 S, 55.325 W)	forest (25 m)	2007–2009

INMET: Brazil's National Institute of Meteorology; FNS: Fazenda Nossa Senhora.

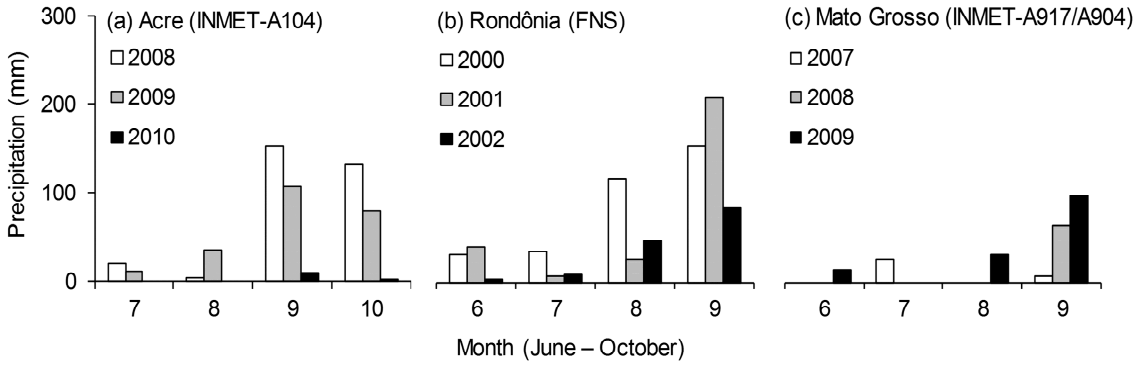

Figure 2. Rainfall measured at weather stations (Acre: INMET-A104, Rondônia: FNS, and Mato Grosso: INMET-A917/A904) during dry season months at three different study sites.

In this study, we utilized ground-based information eddy covariance flux tower data for a comparison to the METRIC ET estimates, daily meteorological data, and Landsat imagery as input data for METRIC (Table 1). Two flux tower sites over the forest region are located at Jaru (Rondônia) and Sinop (Mato Grosso). There was no flux tower measurement available for ET comparisons in Acre. The flux tower in Sinop Mato Grosso is installed over mature tropical semi-deciduous forest with tree heights from 25 m to 28 m [13]. Another flux tower in Jaru, Rondônia, is in dry tropical rainforest over a relatively closed canopy of 30 m height, including emergent trees [7]. The flux tower data in Rondônia (Jaru and Fazenda Nossa Senhora—hereafter FNS) were acquired through the NASA LBA dataset archived at the Oak Ridge National Laboratory Distributed Active Archive Center (http://daac.ornl.gov) with collective datasets provided by [32], whereas the flux tower data from Sinop Mato Grosso was obtained from the study of [13]. Distances between the center of the study area and the flux tower in each site are 43 km and 80 km for Jaru (Rondônia) and Sinop (Mato Grosso), respectively. These flux tower ET data from Rondônia (2000–2002) and Mato Grosso (2007) were used for a daily ET comparison to METRIC-ET estimates for the selected Landsat image dates described in 3.2 below.

All flux tower data include latent heat flux (LE) and sensible heat flux (H) measured by eddy covariance systems. Additionally, meteorological stations installed in each flux tower measured the surface net radiation (R_n), air temperature, air humidity, and wind speed, among other variables. Details about the instrumentation for each site are available in [32] for Jaru and [13] for Sinop.

Hourly meteorological data were obtained from the closest weather station monitored by the National Institute of Meteorology of Brazil (INMET) or from a flux tower located over the pasture region (Table 1). These hourly data were used to compute alfalfa-based reference ET (ET_r) (ASCE-EWRI, 2005) and other necessary inputs for the METRIC processing. A summary of weather data collected from the stations is presented in Table 2.

Table 2. Summary of air temperature, wind speed, and reference ET for the study period.

Weather Station (State)	Year	Tavg	Tmax	Tmin	Wavg	Wmax	Wmin	Avg ET_r	Max ET_r	Min ET_r
INMET-A104 (Acre)	2008	28.30	32.68	17.71	2.47	4.55	1.02	5.01	7.36	0.76
	2009	26.37	31.00	13.23	1.95	4.91	0.63	4.32	7.60	1.14
	2010	26.57	33.29	12.64	1.89	5.52	0.09	4.34	7.97	0.76
FNS (Rondônia)	2000	24.56	28.47	12.96	3.03	9.69	1.37	5.19	8.86	1.70
	2001	24.87	28.74	12.88	2.61	8.00	1.24	5.32	8.95	1.55
	2002	25.69	28.13	20.21	2.75	6.47	1.33	5.31	8.23	1.88
INMET-A917/A904 (Mato Grosso)	2007	27.44	31.40	20.56	2.56	5.05	1.03	5.61	9.28	1.62
	2008	27.54	32.08	20.03	2.43	4.41	0.87	5.69	9.55	0.98
	2009	27.59	31.52	21.98	2.66	4.36	1.10	4.53	7.55	1.17

Tavg, Tmax, and Tmin are average, maximum, and minimum air temperatures (°C); Wavg, Wmax, and Wmin represent average, maximum, and minimum wind speed (m/s); Avg ET_r, Max ET_r, and Min ET_r, are average, maximum, and minimum reference ET (mm/day).

The study focused on capturing ET dynamics associated with potential water stresses during the dry season (June–September). Altogether, 36 Landsat images were selected (Table 3) from Acre (2008–2010), Rondônia (2000–2002), and Mato Grosso (2007–2009) to develop the NDVI indexed METRIC application for the southern Amazon (described in Section 3.2). Based on this approach, the ET variations during the 2009 dry season were analyzed from primary forest, regenerated forest, degraded forest (burned forest), and pasture across the study sites. The selection of study years and periods for comparison to the METRIC ET was determined by the availability of cloud free Landsat images, INMET meteorological data, and flux-tower data, which can be limited for our study region.

Table 3. Landsat image dates for the three study regions used in this study.

Acre			Rondônia			Mato Grosso		
Year	**Image Date**	**Sensor**	**Year**	**Image Date**	**Sensor**	**Year**	**Image Date**	**Sensor**
2008	18-Jul	ETM+	2000	29-Jun *	TM	2007	14-Jun *	TM
	11-Aug	TM		15-Jul *	TM		8-Jul *	ETM+
	12-Sep	TM		16-Aug	TM		9-Aug *	ETM+
	14-Oct	TM		24-Aug *	ETM+		2-Sep *	TM
				17-Sep *	TM			
2009	29-Jul **	TM	2001	8-Jun *	ETM+	2008	16-Jun	TM
	6-Aug **	ETM+		24-Jun *	ETM+		18-Jul	TM
	7-Sep **	ETM+		26-Jul *	ETM+		19-Aug	TM
	1-Oct **	ETM+		19-Aug *	TM		12-Sep	ETM+
				28-Sep	ETM+			
2010	24-Jul	ETM+	2002	11-Jun *	ETM+	2009	19-Jun **	TM
	9-Aug	ETM+		27-Jun *	ETM+		21-Jul **	TM
	26-Sep	ETM+		13-Jul *	ETM+		22-Aug **	TM
	4-Oct	TM		29-Jul *	ETM+		15-Sep **	ETM+
				1-Oct	ETM+			
			2009	14-Jun **	ETM+			
				16-Jul **	ETM+			
				17-Aug **	ETM+			
				26-Sep **	TM			

TM: Thematic Mapper; ETM+: Enhanced Thematic Mapper Plus; * Landsat image date for daily ET comparison between flux tower and METRIC; ** Landsat images used for dry season ET analysis.

3. Methods

3.1. METRIC Evapotranspiration

METRIC is a satellite imagery-based processing model for estimating ET as a residual of the surface energy balance Equation (1) at the earth's surface and is expressed as the energy consumed for evaporation.

$$LE = R_n - G - H \quad (1)$$

where LE = latent energy consumed by ET (W/m^2), R_n = net radiation (W/m^2), G = soil heat flux (W/m^2), and H = sensible heat flux (W/m^2). We briefly summarize the components of the surface energy balance and ET calculation by METRIC below. More details on the METRIC ET estimation procedure are available from [23,24].

R_n represents all incident and reflected short and long wave fluxes and long wave radiant flux emitted from the surface (Equation (2)) and it is computed by subtracting all outgoing radiant fluxes from all incoming radiant fluxes [23,24].

$$R_n = (1 - \alpha)\, RS_i + RL_i - RL_o - (1 - \varepsilon_o)\, RL_o \quad (2)$$

where RS_i and RL_i are incoming shortwave radiation and incoming longwave radiation, respectively. RL_o is outgoing longwave radiation. The surface albedo (α) represents the surface reflectance characteristics and is the ratio of incident radiant flux to reflected radiant flux over the solar spectrum, and ε_o is the broadband surface emissivity.

G is the rate of soil heat flux due to conduction, and is calculated using an empirical equation developed by [33] as:

$$G/R_n = 0.05 + 0.18e^{-0.521LAI} \quad (LAI \geq 0.5) \quad (3a)$$

$$G/R_n = 1.80\,(T_s - 273.16)/R_n + 0.084 \quad (LAI < 0.5) \quad (3b)$$

where LAI is the leaf area index (unitless) and is estimated as a function of SAVI (Soil Adjusted Vegetation Index), as described in [34]. T_s is the surface temperature (Kelvin, K) and is estimated by using a modified Plank equation following [35] with atmospheric and surface emissivity correction [23].

H is the rate of heat flux to air by conduction and convection, and is computed as:

$$H = (\varrho \times c_p \times dT)/r_{ah} \quad (4)$$

where ϱ = air density (kg/m^3), c_p = air specific heat ($J/kg/K$), dT = the temperature difference between two heights (z1 and z2) in a near surface blended layer, and r_{ah} = aerodynamic resistance to heat transport (s/m) between heights z1 and z2.

The calibration of H is accomplished by inverting Equation (4) at two extreme ET conditions present within the image. These extreme ET conditions refer to the wettest and driest conditions and are represented by two anchor pixels, namely a cold pixel (high ET) and a hot pixel (zero or near-zero ET), selected within the image (more description in Section 3.2). Its calibration is based on a linear relationship between the surface temperature (T_s) and dT at two anchor pixels. r_{ah} is estimated during an iterative process based on the friction velocity of the air, the momentum roughness length of the surface, and atmospheric stability [18]. The hot pixel is usually selected from the bare soil surface with a lower Normalized Difference Vegetation Index (NDVI) (<0.20) and higher surface temperature, where the ET rate is assumed to be near zero. The cold pixel is selected from fully covered actively growing agricultural fields which have a lower surface temperature and a high NDVI (>0.75), representing a near potential ET rate [23,24,28].

After computing R_n, G, and H, LE is computed as a residual of the surface energy balance by applying Equation (1). LE is divided by the latent heat of vaporization (λ) to compute instantaneous

ET at the time of satellite overpass. Extrapolation of instantaneous ET (ET_{inst}) to 24-h (daily) ET is obtained by employing the reference ET fraction (ET_rF). ET_rF is synonymous with the well-known crop coefficient (Kc) and is computed as a ratio of ET_{inst} to instantaneous reference ET ($ET_{r\ inst}$) at the satellite overpass time. $ET_{r\ inst}$ is calculated by employing local meteorological data, as detailed in ASCE-EWRI [36]. The instantaneous ET_rF computed at the satellite over pass time is assumed to be equivalent to a 24-hour average [23,36]. The instantaneous ET_rF is then multiplied with daily ET_r to obtain the daily ET.

3.2. METRIC Application in the Southern Amazon

METRIC processing requires four primary inputs: Landsat imagery, local weather data, land cover maps, and Digital Elevation Model (DEM) maps. The Landsat images (Table 3) for this study were downloaded from the USGS Global Visualization Viewer (http://glovis.usgs.gov/). Hourly weather data were collected from weather stations/flux towers over pasture (Table 1) and went through a rigorous quality control process [36,37] to ensure their integrity before computing reference ET (ET_r) and METRIC processing. Land cover maps developed by [38] were used. Elevation maps based on NASA Shuttle Radar Topography Mission (SRTM) data (resampled to 30 m horizontal resolution) were used. Elevation maps were used to adjust the surface temperature and radiation flux as a function of elevation, and land cover maps [38] were used for developing spatial variations in surface roughness.

METRIC utilizes the Calibration using Inverse Modeling at Extreme Conditions (CIMEC) procedure as used in the Surface Energy Balance Algorithm for Land (SEBAL) [18,39] to estimate the dT function (Equation (4)) for the computation of sensible heat flux. The estimation of dT is facilitated by selecting anchor pixels (cold and hot pixels) within the Landsat image. Ideally, cold pixels are selected from agricultural fields with green, actively growing vegetation cover representing the upper end of the ET spectrum within the image. However, in our study in the southwestern Amazon (Acre and Rondônia), pasture regions were considered the most appropriate land use for the selection of cold pixels due to the difficulty in finding suitable agricultural vegetated area [28]. For consistency, cold pixels in Mato Grosso were also selected from fields with pasture even though there were some crop fields observed within the image. These crop fields were used to confirm the final calibration at the cold pixel. Hot pixels were selected from bare soil surface areas with very little vegetation (NDVI < 0.20) representing near zero ET unless residual soil evaporation from antecedent rainfall was present. A bare soil evaporation model [40] was run on a daily time step to adjust for any residual soil evaporation. Additional detail about an iterative process of selecting the cold and hot pixels is described in [28].

ET_rF at the cold pixel is typically assumed to be equivalent to 1.05 [23]. Identifying green pasture for the cold pixel with NDVI > 0.75 during the dry season is challenging. Therefore, the NDVI values of those selected cold pixels were less than that of the ideal cold pixel (>0.75). For this lower NDVI situation, an alternative approach was used to adjust the ET_rF fraction for the cold pixel (Equation (5)) [23,40]. The NDVI-based approximation procedure in (Equation (5)) is commonly applied during non-growing seasons in agricultural settings when the crops are not fully developed, or when the ground is not fully covered by crops. This NDVI indexed approach has been tested during the dry seasons in Rondônia and showed a good agreement with the flux tower ET observations [28].

During the first step (METRIC[1]), we used an empirical equation from [23] as a general approach for agricultural areas in the non-growing season as:

$$ET_rF_{cold} = 1.25 \times NDVI_{cold} \quad (5)$$

where $NDVI_{cold}$ is the NDVI at the cold pixel. This procedure is termed METRIC[1] hereafter.

We also tested a procedure (Equation (6)) suggested by [23] and applied by [26] in the Middle Rio Grande of New Mexico which is based on local data and operator's judgement, for each Landsat scene

in our study region. In Equation (6) (henceforth termed METRIC^2), a linear equation between ET_rF and NDVI was developed at each Landsat sceneto generate new ET_rF_{cold} values for the cold pixels:

$$ET_rF_{cold} = a \times NDVI_{cold} + b \quad (6)$$

where a and b are empirically determined constants, the slope and intercept, for a given linear relationship between ET_rF_{cold} and $NDVI_{cold}$ for each Landsat scene.

To calculate ET_rF_{cold} from these two approaches (Equations (5) and (6)), we first selected fifty 10 by 10-pixel sample polygons (300 m by 300 m) of NDVI from pasture areas at each one of the 36 Landsat images (Table 3). Each sample was located no nearer to the pasture field edges than 90 m to avoid signal contamination within the thermal band during the subsequent processing. From these NDVI samples, the top 20% NDVI (10 samples) from each image was further selected as a representation of potential samples for the selection of the cold pixel. For the METRIC^1 procedure, a suitable cold pixel was selected from the top 20% NDVI samples for each image and Equation (4) was applied for complete METRIC processing. For the METRIC^2 approach, the ET_rF values (ET_rF^1) obtained from METRIC^1 were integrated with the top 20% NDVI samples to develop linear regression equations at each Landsat scene. To generate this NDVI-ET_rF equation, the ET_rF^1 values corresponding to the top 20% NDVI samples were extracted and averaged for each image date (Table 4). One image from each month was selected during the dry season months to cover the seasonal NDVI variations across the study sites. The linear relationship at each Landsat scene was developed using 12 data points (for 12 image dates). These new developed equations for each Landsat scene were applied for the complete processing of the METRIC^2 approach. While the cold pixel was the same for these two different METRIC approaches for the same image date, the ET_rF_{cold} values were different, depending on the equation used (Equations (5) and (6)). The unique set of cold and hot pixels was selected for each image date and iterative post-processing was completed until a suitable set of anchor pixels were identified.

Table 4. Relationships between METRIC ET estimated by two different approaches and flux tower ET in Jaru (Rondônia) and Sinop (Mato Grosso).

Statistical Parameters	Jaru (Rondônia)		Sinop (Mato Grosso)		Overall	
	METRIC [1]	METRIC [2]	METRIC [1]	METRIC [2]	METRIC [1]	METRIC [2]
RMSE	0.81	0.38	0.61	0.24	0.77	0.35
MAPE	20	9	16	6	19	8
R^2	0.66	0.72	0.82	0.77	0.70	0.73
Slope *	1.07 (0.54, 1.60)	1.05 (0.58, 1.51)	1.50 (0.65, 3.65)	1.14 (0.77, 3.06)	1.14 (0.71, 1.56)	1.12 (0.73, 1.50)
Intercept *	0.44 (−1.55, 2.42)	−0.04 (−1.79, 1.70)	−1.13 (−8.48, 6.21)	−0.65 (−7.19, 5.89)	0.17 (−1.38, 1.72)	−0.36 (−1.78, 1.06)

RMSE: Root Mean Squared Error (mm/day); MAPE: Mean Absolute Percentage Error (%); [1] METRIC ET results with ET_rF_{cold} = 1.25 $NDVI_{cold}$; [2] METRIC ET results with ET_rF_{cold} from new developed equations; * Upper and lower 95% confidence interval.

For the application of METRIC in Amazonian forest, some adjustments were made such as improvements for the estimation of surface roughness length (zom) and surface temperature (T_s), as described in [28]. To improve the zom estimation across multiple forest types, the zom estimation method by [41] was used. The Perrier zom estimation is based on LAI, average tree height, and vertical canopy distribution. The zom values for multiple forest types such as primary forest, regenerated forest, and degraded forest (Mato Grosso only), were calculated. The heights of primary and regenerated forests were considered to be 30 m and 20 m, respectively, and degraded forests were 15 m. The canopy distribution was assumed to be uniform for primary and regenerated forests, and sparsely topped canopy for degraded forests. The maximum value of zom for each forest type was limited to 1.0 m. To account for the potential T_s reduction due to shadow impacts on albedo resulting from differences in the sun angle to that of the nadir-viewing satellite in tall vegetation, a linear adjustment on ET_rF

based on the surface albedo, NDVI, T_s, and ET_rF of the hot and the cold pixels was made [34]. However, due to a small impact of T_s adjustment (i.e., <2%) on the final forest ET, the standard method of T_s estimation within the METRIC procedure was followed in this study.

3.3. Comparison to Flux-Tower ET Estimates

Daily forest ET data from the METRIC procedure (METRIC^1 and METRIC^2) were compared to flux tower ET data. A common challenge with flux tower ET is the lack of energy balance closure [42,43]; therefore, comparisons were only made with the energy balance closure (EBC) ratio $(H + LE)/(R_n - G)) \geq 0.80$. In other words, METRIC and flux tower ET were only compared on days with an EBC error of less than 20%. For the comparable image days, energy balance closure errors ($R_n - H - LE - G$) in flux tower data were distributed between H and LE by applying the constant Bowen-ratio approach [42] to compute the daily ET from the flux tower. ET data from METRIC were extracted by taking three different pixel window sizes (3×3, 5×5, and 9×9) centered on the flux tower location to identify the appropriate sampling area. The ET comparisons showed less (within 0.2 mm/day) variation among these sampling units, indicating homogeneous land covers around the flux towers; therefore, 3×3 pixel window was chosen for comparisons and analysis [28].

The errors and accuracy estimation between the METRIC procedures (METRIC^1 and METRIC^2) and flux tower ET were made by computing the root mean square error (RMSE) and mean absolute percentage error (MAPE) as:

$$\text{RMSE} = \sqrt{\frac{\sum_{i=1}^{n} (\text{METRIC ET} - \text{fluxtower ET})^2}{n}} \quad (7)$$

$$\text{MAPE} = \frac{1}{n} \sum_{i=1}^{n} \text{abs}\left(\frac{\text{METRIC ET} - \text{fluxtower ET}}{\text{fluxower ET}} \right) \text{x } 100 \quad (8)$$

where METRIC ET is the ET estimated from METRIC and flux-tower ET from flux tower observations, and n is the number of days available for comparison. The agreement between the daily flux-tower ET and METRIC ET was tested by the coefficient of determination (R^2) of a linear regression line.

3.4. Characterization of Dry Season ET Patterns from Different Land Cover Types in the Southern Amazon

The METRIC^2 approach was applied to estimate ET from different land cover types including intact forest, regeneration, degraded (burned forest) forest, and pasture to characterize their variation during the dry season of the year 2009 across three study sites as a further improvement of the NDVI-indexed ET estimation. Dry seasons at the study sites usually last for three to five months; however, the dry season ET comparison and analysis were made from July to September to be consistent with the time period across all study sites. Daily ET estimates were obtained as a product of daily ET_rF^2 (from EMTRIC^2) and corresponding ET_r. The ET_rF^2 values between the satellite overpass dates were obtained by spline interpolation. The average monthly ET was computed as a simple division of the monthly ET (sum of daily ET) by the number of days for the specific month. The average monthly ET rates from each land cover type were computed by taking averaged values of 10 samples from each land cover type within a Landsat scene. Each sample was 10 by 10 pixels and selected so as to cover the spatial distribution of each land cover type within an image.

Identification of primary forest, regenerated forest, degraded forest (only in Mato Grosso), and pasture land cover types within a satellite image was made with references from the land cover products "TerraClass" [44] and forest degradation products by the Brazil's National Institute for Space Research (INPE-DEGRAD) [31]. The INPE TerraClass is available for 2008, 2010, and 2012 as of the time of our analysis (http://www.inpe.br/cra/ingles/project_research/terraclass.php). To confirm the same land cover type for our study year 2009, we considered the TerraClass products of the years 2008 and 2010. For degraded forest (burned forests) in Mato Grosso, INPE DEGRAD data (INPE, 2016) was used for 2009.

Statistical analyses of dry season ET from different land covers were made by applying one-way analysis of variance (ANOVA) and student's t-test at the 5% significance level.

4. Results

4.1. NDVI vs ET$_r$F Relationship

The pastures in our study regions are rain-fed and usually at various stages of senesce in the dry season [45]. The NDVI results from all selected Landsat image dates for each scene were lower than 0.75 and indicated an overall decreasing trend of pasture greenness as the dry season proceeded at all study sites (Figure 3). The highest intensity and longest duration of pasture dryness was observed in Mato Grosso as compared to Rondônia and Acre. The largest differences of pasture greenness during the later dry season in each region are mainly attributed to pasture responses to increased rainfall (Figure 2).

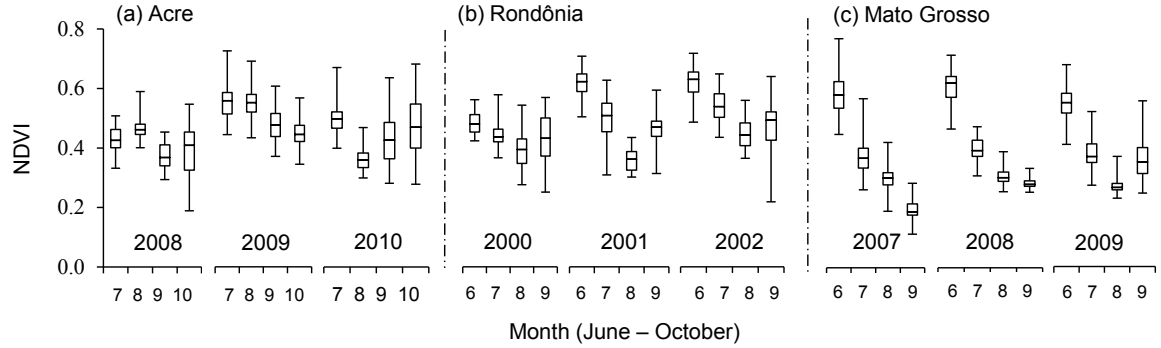

Figure 3. Variation in NDVI during the dry season among selected 50 samples at each site.

The linear relationships between ET$_r$F[1] and NDVI from the selected NDVI pasture samples at each site are shown in Figure 4. The averaged NDVI values from the samples varied between 0.24 and 0.67. The lowest top-end NDVI value at Acre was 0.31 (DOY 221, 2010) and highest of 0.62 (DOY 210, 2009). At Rondônia, NDVI varied from 0.38 (DOY 231, 2001) to 0.66 (DOY 162, 2002), and between 0.24 (DOY 245, 2007) and 0.67 (DOY 165, 2007) at Mato Grosso. The average ETrF[1] (from METRIC[1]) values were between 0.27 and 0.78 across the study sites.

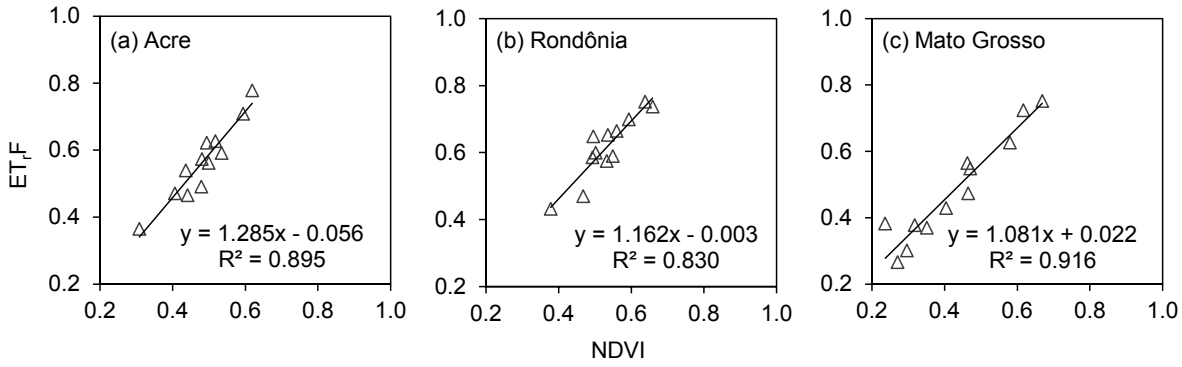

Figure 4. ET$_r$F vs. NDVI relationships from pasture samples at all study sites. Each triangle point represents the averaged values of ET$_r$F[1] (from METRIC[1]) and NDVI for each one of the selected satellite image dates for the top 20% of NDVI samples.

The ET$_r$F and NDVI relationships (Figure 4) indicated the lowest regression line slope in Mato Grosso (1.081) and the greatest in Acre (1.285). These results showed distinct pasture phenological changes

across the study regions during the dry season. The coefficient of determination (R^2) was between 0.83 and 0.92. In Mato Grosso, NDVI and ET_rF tended to follow a 1:1 relationship, whereas the ET_rF values increased towards the southwest following the Rondônia and Acre regions. These trends indicate greater pasture ET rates from the southwest Amazon region compared to Mato Grosso under similar NDVI conditions.

4.2. METRIC ET from Variable ET_rF and Comparison to Flux-Tower Measurements

The ET rates estimated using either METRIC method were higher than the ET from flux tower measurements (Figure 5). The comparable image dates were limited (12 dates at Jaru Rondônia and four dates at Sinop Mato Grosso) due to the availability of both cloud free Landsat images and good quality flux tower data. Flux tower data often lags energy balance closure (EBC) [42,43]. A study by [43] reported a mean EBC error from the flux tower in the order of 20% based on 50 site-years across 22 sites over multiple vegetation covers. This is not different in the case of our study. The EBC errors at Jaru were 33%, 30%, and 25% during the study periods in the year 2000, 2001, and 2002, respectively. At Sinop in 2007, the EBC error was 12%.

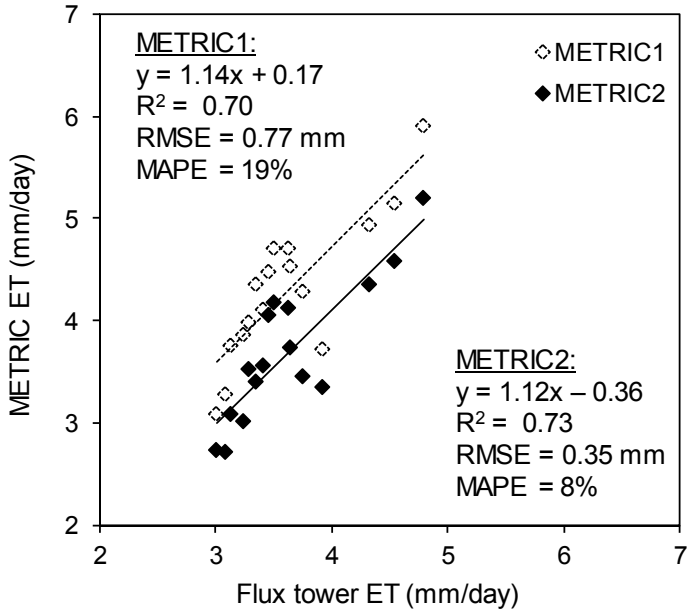

Figure 5. Overall comparison of flux-tower ET and METRIC ET obtained from Jaru Rondônia (2000–2002) and Sinop Mato Grosso (2007) by two different approaches.

At both of the flux tower sites (Jaru-Rondônia and Sinop-Mato Grosso), $METRIC^2$ provided lower RMSE and lower MAPE values (Table 4), indicating a better performance than $METRIC^1$ procedure when compared with the flux tower observations. At Jaru, RMSE lowered from 0.81 mm/day to 0.38 mm/day, while this error reduction was from 0.61 mm/day to 0.24 mm/day at Sinop. The MAPE values were less than 10% from the $METRIC^2$ approach. Overall, there was a slight increase in the R^2 value (0.70 to 0.73), but a greater decrease in RMSE (from 0.77 to 0.35 mm/day) and MAPE (19% to 8%) with $METRIC^2$ compared to $METRIC^1$ (Table 4). The absolute mean difference also decreased to ±0.28 mm/day from ±0.69 mm/day.

4.3. Dry Season ET Patterns across Different Land Cover Types

Primary forest shows high NDVI and ET_rF values in Acre and Rondônia, while in Mato Grosso, a lower ET_rF value is observed and the differences between NDVI and ET_rF become larger in the later dry season (Figure 6a). A similar trend is found with regenerated forest (Figure 6b). The differences

between NDVI and ET_rF tend to be larger during the dry season in regenerated forest in all three sites. Pasture showed much lower NDVI and ET_rF values, but the differences between these variables were smaller compared to regenerated forests (Figure 6c). T_s tend to be higher in pasture than forests and the surface albedo stayed constant during the dry season in all three sites.

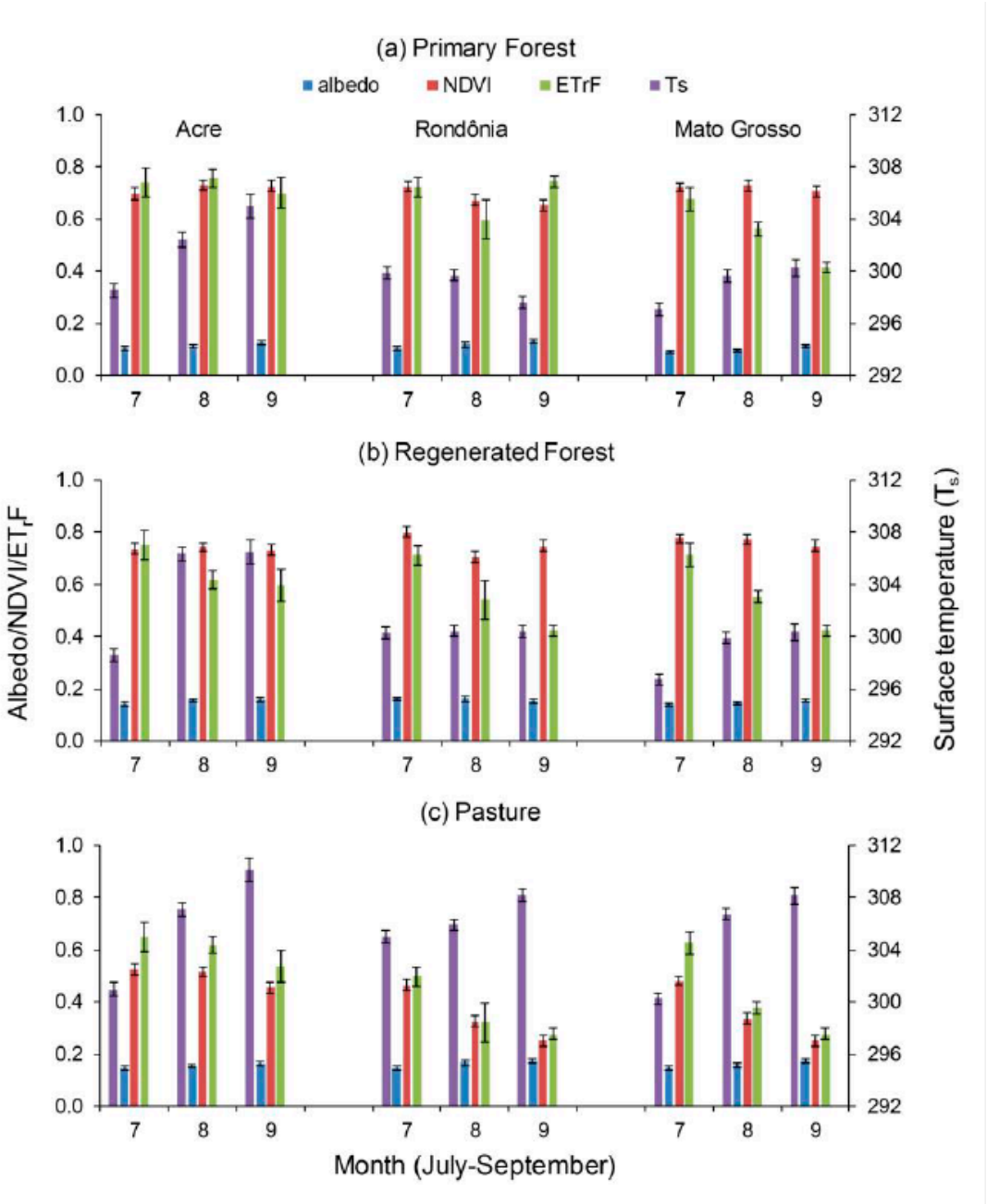

Figure 6. Variation of surface temperature, albedo, NDVI, and ET_rF from primary forests, regenerated forests, and pasture during the dry season in 2009 in the study sites.

Variations in monthly ET rates estimated by METRIC^2 for different land cover types during the 2009 dry season are illustrated in Figure 7. Among the three study sites, Mato Grosso showed the lowest ET rates from all land cover types in Mato Grosso (Figures 7 and 8 and Table 5) compared to Rondônia and Acre.

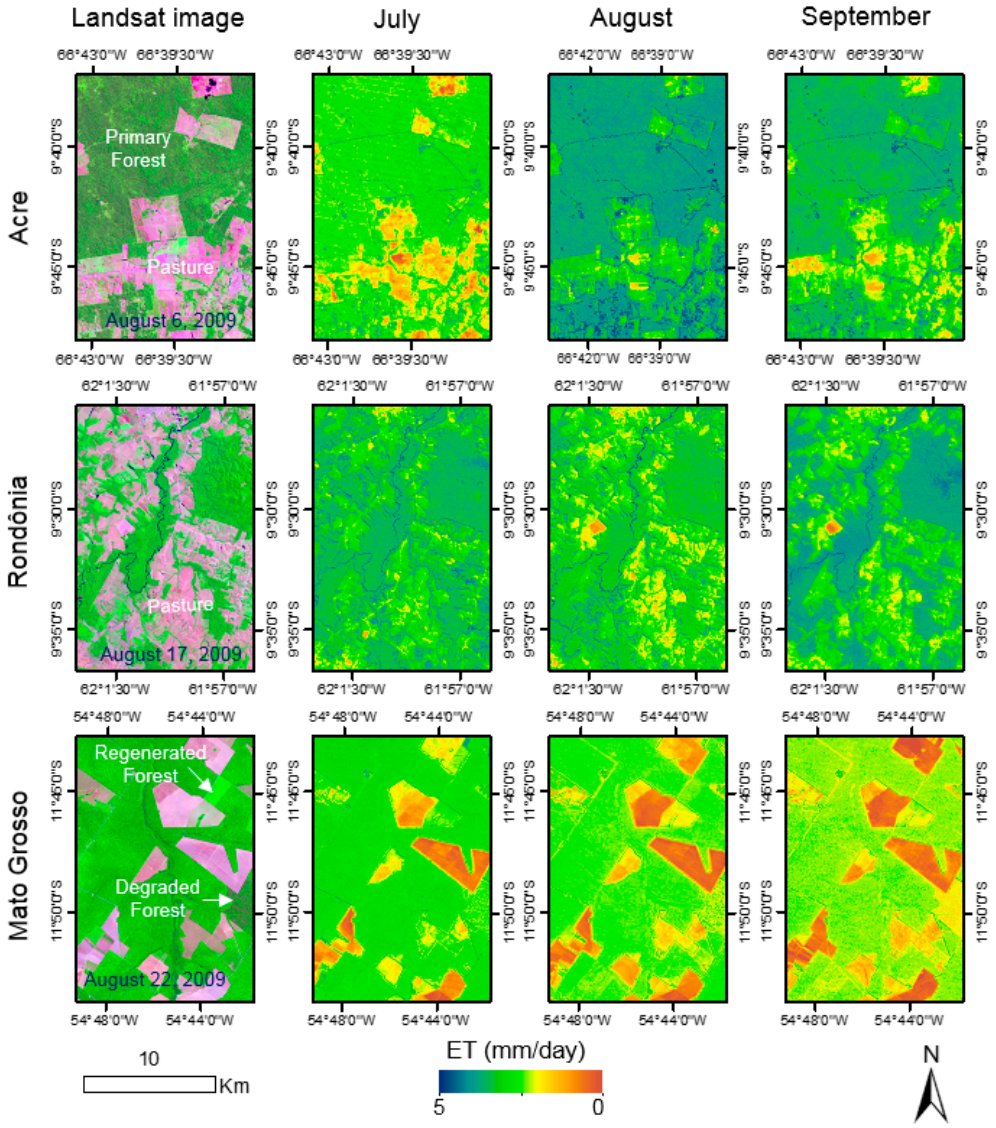

Figure 7. Monthly ET variations from different land cover types during July, August, and September across the study sites in 2009.

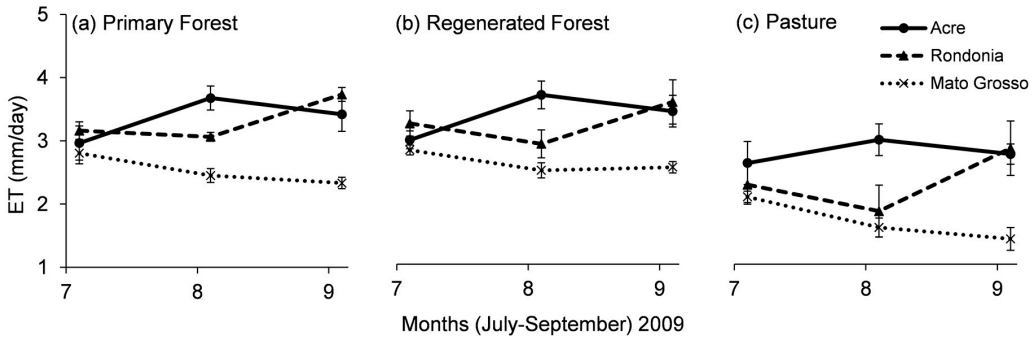

Figure 8. ET rates of (**a**) primary forest; (**b**) regenerated forest; and (**c**) pasture from three sites during the dry season (July–September) of 2009 at each study site.

For primary forest, the monthly ET rates for the three sites were at the same level in the early dry season and increased towards September in Acre and Rondônia, whereas an opposite pattern

was observed in Mato Grosso (Figure 8a). Thus, the highest monthly ET rate was recorded in July (2.81 mm/day) in Mato Grosso, August (3.68 mm/day) in Acre, and September (3.73 mm/day) in Rondônia. The lowest monthly ET rates from primary forest were observed in July (2.97 mm/day), August (3.06 mm/day), and September (2.33 mm/day) in Acre, Rondônia, and Mato Grosso, respectively. The dry season average ET from primary forest in Acre and Rondônia was similar, with values of 3.35 mm/day and 3.32 mm/day, respectively, while Mato Grosso presented the lowest ET rate (2.53 mm/day), which was statistically different from the other sites (Table 5). The largest variation in monthly average ET rates was observed in Acre (0.71 mm/day), followed by Rondônia (0.67 mm/day), and drier Mato Grosso (0.47 mm/day).

Table 5. Summary of statistical significance (*p*-value) of mean dry season ET comparison between the three study sites and different land covers.

Site-to-Site Comparison		Acre-Rondônia	Rondônia-Mato Grosso	Mato Grosso-Acre
Land Cover	Primary Forest	0.928	<0.0001	<0.0001
	Regenerated Forest	0.982	<0.0001	<0.0001
	Pasture	0.006	<0.0001	<0.0001

Dry season ET patterns of regenerated forest were similar to those observed in primary forest in the three study regions (Figure 8b). The dry season average ET rates from regenerated areas were 3.22 mm/day in Acre, 3.23 mm/day in Rondônia, and 2.61 mm/day in Mato Grosso. These ET rates in Acre and Rondônia were slightly lower compared to primary forest, but exhibited a higher dry season average ET than primary forest in Mato Grosso. However, these differences between regenerated and primary forests in ET at each site were not statistically significant (Table 6). Similar to primary forest, the peak monthly ET rates from regenerated forest were in August (3.48 mm/day), September (3.57 mm/day), and July (2.81 mm/day) in Acre, Rondônia, and Mato Grosso, respectively. Monthly ET rates were statistically similar between Acre and Rondônia; however, they were different in Mato Grosso (Table 5). The variations in the monthly average rates from regenerated forest were lower than those from primary forest at all study sites. These results from our study indicated that both primary and regenerated forests showed greater responses to rainfall in relatively drier (low rainfall) Mato Grosso (Figures 8 and 9).

Pasture showed significantly lower ET rates compared with primary and regenerated forests in all three study sites over the dry season (Figure 8c and Table 6). Variations in ET were larger for Mato Grosso and Rondônia than for Acre (Figure 8c). There was a declining trend in pasture ET from July to September in Mato Grosso, whereas subtle changes in pasture ET during the same period in Acre. Monthly pasture ET rates in Rondônia varied more strongly compared to the other sites, and ET declined in August and increased to 2.83 mm/day in September. Pasture ET rates in these sites range between 1.40 mm/day in September in Mato Grosso and 2.97 mm/day in August in Acre. The dry season average ET rate in Mato Grosso (1.68 mm/day), the driest region, was significantly lower (p-value < 0.05) than Rondônia (2.31 mm/day) and Acre (2.77 mm/day) during the dry season (Table 5). These statistical comparisons show that ET from pasture varies significantly during the dry seasons.

Table 6. A summary of the statistical comparison of monthly and dry season ET from different land cover types within each study site for July (J), August (A), and September (S).

Land Cover-Wise Comparison/Dry Season Months	Pasture-Regenerated Forest				Pasture-Primary Forest				Regenerated Forest-Primary Forest			
	J	A	S	DS	J	A	S	DS	J	A	S	DS
Acre	*	*	*	*	*	*	*	*	±	±	±	±
Rondônia	*	*	*	*	*	*	*	*	±	±	±	±
Mato Grosso	*	*	*	*	*	*	*	*	±	±	*	±

DS = dry season; * statistically significant (p-value < 0.05); ± statistically not significant (p-value > 0.05).

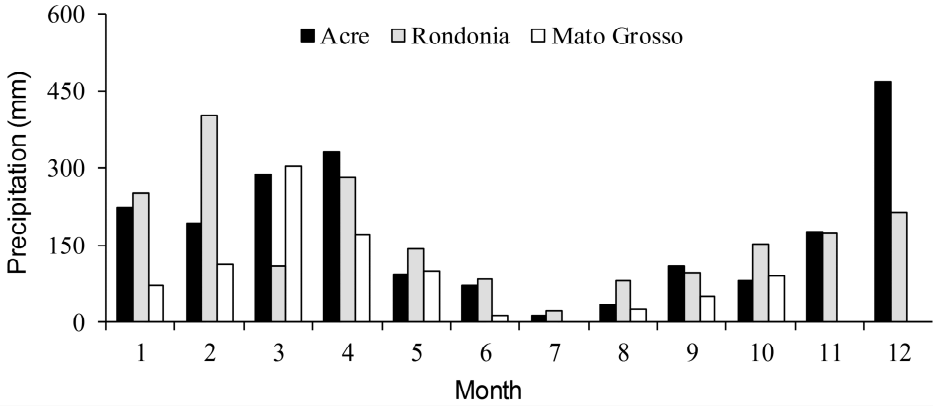

Figure 9. Monthly precipitation across study sites in 2009 from INMET. Note: Precipitation data from July, November, and December for Mato Grosso are missing.

Degraded forest exists only in Mato Grosso in this study. Dry season ET rates from three different forest cover types (primary, regenerated, degraded) showed different ET trends (Figure 10). Monthly ET rates from degraded forest in Mato Grosso were lower than both primary forest and regenerated forest and showed a continuously declining trend, which was similar to pasture (Figure 10). The lowest ET was in September (1.50 mm/day), which was close to the pasture ET (1.40 mm/day) for the same month. Unlike regenerated forests, degraded forests did not show increased ET in response to increased rainfall during the later dry season (Figures 8 and 9). The monthly average ET rates from degraded forest were less than 2.50 mm/day during dry season months. The dry season average ET from degraded forest (2.03 mm/day) was significantly different (p-value < 0.05) than that from regenerated (2.61 mm/day) and primary forest (2.53 mm/day) in Mato Grosso.

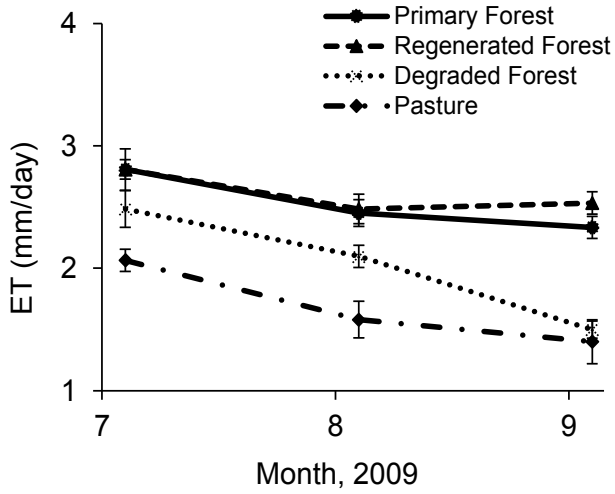

Figure 10. Dry season ET from the three different forest categories and pasture in Mato Grosso.

5. Discussion

Spatially explicit and higher resolution information such as 30 m from Landsat imagery is necessary to analyze the effect of land cover type on ET and the impact of disturbances on the water balance in fragmented forest ecosystems in the Amazon. In this study, we addressed two main issues: (1) adaptation of METRIC to the southern Amazon region; and (2) characterization of fine spatial scale, dry season ET dynamics from different land cover types in this region.

5.1. Adaptation of METRIC to the Amazon

We applied an empirical relationship between NDVI and ET_rF to calibrate H, which is different from the standard METRIC approach. Distinct regression relationships (greater ET_rF values towards the southwest Amazon region) between ET_rF and pasture NDVI were found from METRIC^2 across the study regions (Figure 4), which were related to how ET varied in response to local climatology [6]. These results indicate the need for regionally suitable linear equations to estimate ET_rF_{cold} to account for ET variation with climate across the study regions. While identifying a suitable cold pixel is challenging when applying the METRIC procedure in the Amazon region [28], the linear relationships developed in this study help provide a guidance for adapting the model in similar hydro-climatic regions. The METRIC^2 approach showed improved correlations with tower-measured ET compared to METRIC^1 with lower errors (Table 4). Our results show that METRIC with the NDVI indexed ET_rF approach can provide ET estimates, even in places where there is difficulty in finding an ideal cold pixel (NDVI $\geq$ 0.75) as opposed to the standard approach that requires this criterion for the cold pixel selection. The same approach has been tested in the Middle Rio Grande of New Mexico with MODIS at the 1000 m coarser ground-resolution, in which the identification of a cold pixel with a uniform full vegetation cover was very challenging [26].

Numata et al. [28] discuss other challenges related to satellite-based ET estimations in the Amazon, including uncertainties in estimating the surface resistance (zom) and surface temperature, a limited weather station network, and the availability of cloud free Landsat data. In this study, we selected three sites based upon the availability of both meteorological data and cloud free Landsat data.

5.2. Dry Season ET Dynamics

The overall ET trends and variations are strongly influenced by rainfall and the dry season length. Mato Grosso presents the lowest monthly precipitation during the dry season and shows significantly low dry season ET from all land cover types compared to the other sites (Table 5, Figure 8). Its precipitation during the 2009 dry season (74 mm) was 50% compared to Acre (156 mm) and Rondônia (200 mm), which indicates severe water stress conditions. Furthermore, with a longer dry season with an earlier start in Mato Grosso (i.e., May to September vs. June to September in in Acre and Rondônia), its landscape is exposed to even higher water stress conditions, such as low soil water storage and a low relative humidity, and results in a progressively declining ET trend even though the precipitation increased in September (Figure 8). The other two regions showed the recovery of ET from the studied land cover types during the dry season. These regional patterns of ET for primary forest are consistent with those estimated by flux tower-based measurements [6,7,13]. For example, in terms of the dry season ET rates from primary forests, our ET rates estimated by METRIC for Rondônia (3.32 mm/day) are similar to those obtained by [7] between 3.22 mm/day to 3.35 mm/day, based on multiple data filtering.

Distinct ET trends from land cover types are linked to their biophysical properties such as the leaf area index (LAI) and root system. Primary and regenerated forests withdraw water from the deep profile of soil due to its deep root systems [32,46,47]. Juarez et al. [47] reported that soil water storage within the top 3m layer was sufficient to maintain a stable ET rate in forest areas in Rondônia. Therefore, forests are resistant to water stress and their ETs are stable even during the normal dry season. In contrast, pasture with a shallow root system and higher albedo suffers from water stress more severely than forest and exhibits more variable ET dynamics in the dry season [32]. While the areas of secondary and degraded forests are expanding in the Amazon [47,48], ET and its seasonal dynamics from these forests are still highly uncertain. We did not estimate significant differences in ET between primary and regenerated forests at all sites (Table 6), but the rates of ET from regenerated forests may vary in time and space due to the biophysical conditions of regenerated forest associated with its age, plant density, and species composition. Regarding degraded forest, ET from degraded or burned forest in Mato Grosso was much lower than that from primary and regenerated forest as transpiration is limited by the loss of leaves from trees in the degraded area [49]. However,

like regenerated forest, ET from degraded forests are highly variable depending upon their biophysical conditions such as the leaf area index (LAI) and above ground biomass associated with degradation type (e.g., logging and fire) and intensity, as well as the time after disturbance [50,51].

6. Conclusions

We studied the ET dynamics from critical land cover types in Acre, Rondônia, and Mato Grosso in the southern Amazon during the dry season (July–September) using spatially explicit ET data estimated using the Landsat-based METRIC model. This model, widely used for agricultural fields, was adapted to Amazonian ecosystems using a linear relationship between NDVI and ET_rF that varies regionally [26]. This approach improved the model performance for ET estimations in the southern Amazon. RMSE was reduced from 0.77 mm/day to 0.35 mm/day, the absolute mean difference from $\pm$0.69 to $\pm$0.28 mm/day, MAPE from 19% to 8%, and R^2 from 0.70 to 0.73, when compared to daily flux tower ET measurements.

ET dynamics from primary, regenerated, and degraded forests and pasture at the three study sites in the southern Amazon during the dry season showed variable responses from different land cover types to water stress at the landscape level. The ability to map high-resolution ET is key for understanding the water cycle and stress over fragmented ecosystems with forests at different stages of degradation and recovery in the Amazon. Our results indicate that the higher resolution METRIC ET maps developed here can be effective for studying spatial and temporal variations in ET over human-impacted landscapes with variable forest conditions and could potentially be used for areas outside of the Amazon.

Acknowledgments: This work is supported by a research grant from the NASA Terrestrial Ecology Program (NNH13ZDA001N-TE). We greatly acknowledge the use of LBA flux tower data for the model comparisons and weather station data from INMET (Brazil's National Institute of Meteorology).

Author Contributions: Kul Khand, Izaya Numata, and Jeppe Kjaersgaard conceived and designed the experiment. Kul Khand and Izaya Numata prepared and processed the METRIC data, while George Vourlitis processed the flux-tower data. Izaya Numata, Kul Khand, Jeppe Kjaersgaard, and George Vourlitis contributed to the analysis and the interpretation of the results. Kul Khand and Izaya Numata wrote the paper and all the other members revised the paper.

Conflicts of Interest: The authors declare no conflict of interest. And the founding sponsors had no role in the design of the study; in the collection, analyses, or interpretation of data; in the writing of the manuscript, and in the decision to publish the results.

References

1. Salati, E.; Nobre, C.A. Possible climatic impacts of tropical deforestation. *Climat. Chang.* **1991**, *19*, 177–196. [CrossRef]
2. Dias, M.A.F.S.; Rutledge, S.; Kabat, P.; Dias, P.L.S.; Nobre, C.; Fisch, G.; Dolman, A.J.; Zipser, E.; Garstang, M.; Manzi, A.O. Cloud and rain processes in a biosphere-atimosphere interactions context in the Amazon region. *J. Geophys. Res.* **2002**, *107*, 8072. [CrossRef]
3. Choudhury, B.J.; DiGirolamo, N.E.; Susskind, J.; Darnell, W.L.; Gupta, S.K.; Asrar, G. A biophysical process-based estimate of global land surface evapotranspiration using satellite and ancillary data II. Regional and global patterns of seasonal and annual variations. *J. Hydrol.* **1998**, *205*, 186–204. [CrossRef]
4. Dirmeyer, P.A.; Brubaker, K.L. Characterization of the global hydrologic cycle from a back-trajectory analysis of atmospheric water vapor. *J. Hydrometeorol.* **2007**, *8*, 20–37. [CrossRef]
5. Nepstad, D.C.; Decarvalho, C.R.; Davidson, E.A.; Jipp, P.H.; Lefebvre, P.A.; Negreiros, G.H.; Dasilva, E.D.; Stone, T.A.; Trumbore, S.E.; Vieira, S. The role of deep roots in the hydrological and carbon cycles of amazonian forests and pastures. *Nature* **1994**, *372*, 666–669. [CrossRef]
6. Hasler, N.; Avissar, R. What controls evapotranspiration in the amazon basin? *J. Hydrometeorol.* **2007**, *8*, 380–395. [CrossRef]

7. Costa, M.H.; Biajoli, M.C.; Sanches, L.; Malhado, A.C.M.; Hutyra, L.R.; da Rocha, H.R.; Aguiar, R.G.; de Araujo, A.C. Atmospheric versus vegetation controls of Amazonian tropical rain forest evapotranspiration: Are the wet and seasonally dry rain forests any different? *Geophys. Res.* **2010**, *115*, G04021. [CrossRef]
8. da Rocha, H.R.; Manzi, A.O.; Cabral, O.M.; Miller, S.D.; Goulden, M.L.; Saleska, S.R.; Coupe, N.R.; Wofsy, S.C.; Borma, L.S.; Artaxo, P.; et al. Patterns of Water and Heat Flux across a Biome Gradient from Tropical Forest to Savanna in Brazil. *J. Geophys. Res.* **2009**, *114*, G00B12. [CrossRef]
9. Harper, A.; Baker, I.T.; Denning, A.S.; Randall, D.A.; Dazlich, D.; Branson, M. Impact of evapotranspiration on dry season climate in the amazon forest. *J. Clim.* **2014**, *27*, 574–591. [CrossRef]
10. Shukla, J.; Nobre, C.A.; Sellers, P.J. Amazon deforestation and climate change. *Science* **1990**, *247*, 1322–1325. [CrossRef] [PubMed]
11. Werth, D.; Avissar, R. The local and global effects of Amazon deforestation. *J. Geophys. Res.* **2002**, *107*. [CrossRef]
12. Spracklen, D.V.; Arnold, S.R.; Taylor, C.M. Observations of increased tropical rainfall preceded by air passage over forests. *Nature* **2012**, *489*, 282–285. [CrossRef] [PubMed]
13. Vourlitis, G.L.; Nogueira, J.S.; Lobo, F.A.; Pinto, O.B. Variations in evapotranspiration and climate for an Amazonian semi-deciduous forest over seasonal, annual, and El Niño cycles. *Int. J. Biometeorol.* **2015**, *59*, 217–230. [CrossRef] [PubMed]
14. Wright, I.R.; Gash, J.H.C.; da Rocha, H.R.; Shuttleworth, W.J.; Nobre, C.A.; Maitelli, G.T.; Zamparoni, C.A.G.P.; Carvalho, P.R.A. Dry season micrometeorology of central Amazonian ranchland. *Q. J. R. Meteorol. Soc.* **1992**, *118*, 1083–1099. [CrossRef]
15. Vourlitis, G.L.; Filho, N.P.; Hayashi, M.M.S.; Nogueira, J.S.; Caseiro, F.T.; Campelo, J.H. Seasonal variations in the evapotranspiration of a transitional tropical forest of Mato Grosso, Brazil. *Water Resour. Res.* **2002**, *38*. [CrossRef]
16. Vourlitis, G.L.; Nogueira, J.S.; Lobo, F.D.; Sendall, K.M.; de Paulo, S.R.; Dias, C.A.A.; Pinto, O.B.; de Andrade, N.L.R. Energy balance and canopy conductance of a tropical semi-deciduous forest of the southern Amazon Basin. *Water Resour. Res.* **2008**, *44*, W03412. [CrossRef]
17. Jackson, R.D.; Moran, M.S.; Gay, L.W.; Raymond, L.H. Evaluating evapotranspiration from field crops using airborne radiometry and ground-based meteorological data. *Irrg. Sci.* **1987**, *8*, 81–90.
18. Bastiaanssen, W.G.M.; Menenti, M.; Feddes, R.A.; Holtslag, A.A.A. A remote sensing surface energy balance for land (SEBAL). 1. Formulation. *J. Hydrol.* **1998**, *212*, 198–212. [CrossRef]
19. Allen, R.G.; Tasumi, M.; Morse, A.; Trezza, R.; Wright, J.; Bastiaanssen, W.; Kramber, W.; Lorite, I.; Robison, C. Atellite-Based Energy Balance for Mapping Evapotranspiration with Internalized Calibration (METRIC)—Applications. *J. Irrig. Drain. Eng.* **2007**, *133*, 395–406. [CrossRef]
20. Anderson, M.C.; Kustas, W.P.; Norman, J.M.; Hain, C.R.; Mecikalski, J.R.; Schultz, L.; Gonzalez-Dugo, M.P.; Cammalleri, C.; d'Urso, G.; Pimstein, A.; et al. Mapping daily evapotranspiration at field to continental scales using geostationary and polar orbiting satellite imagery. *Hydrol. Earth Syst. Sci.* **2011**, *15*, 223–239. [CrossRef]
21. Mu, Q.; Heinsch, F.A.; Zhao, M.; Running, S.W. Development of a global evapotranspiration algorithm based on modis and global meteorology data. *Remote Sens. Environ.* **2007**, *111*, 519–536. [CrossRef]
22. Mu, Q.Z.; Zhao, M.S.; Running, S.W. Improvements to a modis global terrestrial evapotranspiration algorithm. *Remote Sens. Environ.* **2011**, *115*, 1781–1800. [CrossRef]
23. Allen, R.G.; Tasumi, M.; Trezza, R. Satellite-Based energy balance for Mapping Evapotranspiration with Internalized Calibration (METRIC)—Model. *J. Irrig. Drain. Eng.* **2007**, *133*, 380–394. [CrossRef]
24. Allen, R.G.; Irmak, A.; Trezza, R.; Hendrickx, J.M.H.; Bastiaanssen, W.; Kjaersgaard, J. Satellite-based ET estimation in agriculture using SEBAL and METRIC. *Hydrol. Process.* **2011**, *25*, 4011–4027. [CrossRef]
25. Santos, C.; Lorite, I.J.; Allen, R.G.; Tasumi, M. Aerodynamic parameterization of the satellite-based energy balance (METRIC) model for ET estimation in rainfed olive orchards of Andalusia, Spain. *Water Resour. Manag.* **2012**, *26*, 3267–3283. [CrossRef]
26. Trezza, R.; Allen, R.G.; Tasumi, M. Estimation of actual evapotranspiration along the Middle Rio Grande of New Mexico using MODIS and Landsat imagery with the METRIC model. *Remote Sens.* **2013**, *5*, 5397–5423. [CrossRef]

27. Bhattarai, N.; Quackenbush, L.J.; Dougherty, M.; Marzen, L.J. A simple Landsat-MODIS fusion approach for monitoring seasonal evapotranspiration at 30 m spatial resolution. *Int. J. Remote Sens.* **2015**, *36*, 115–143. [CrossRef]
28. Numata, I.; Khand, K.; Kjaergaard, J.; Cochrane, M.A.; Silva, S.S. Evaluation of Landsat-based METRIC modeling to provide high-spatial resolution evapotranspiration estimates for Amazonian forests. *Remote Sens.* **2017**, *9*, 46. [CrossRef]
29. Numata, I.; Cochrane, M. Forest fragmentation and its potential implication in the Brazilian Amazon between 2001 and 2010. *Open J. For.* **2012**, *2*, 265–271. [CrossRef]
30. Vedovato, L.B.; Fonseca, M.G.; Arai, E.; Anderson, L.O.; Aragão, L.O.C. The extent of 2014 forest fragmentation in the Brazilian Amazon. *Reg. Environ. Chang.* **2016**, *16*, 2485. [CrossRef]
31. INPE. Monitoramento da covertura florestal da Amazônia por satélites. Sistemas PRODES, DETER, DEGRAD e Queimadas 2007–2008. Available online: http://www.obt.inpe.br/prodes/Relatorio_Prodes2008.pdf (accessed on 1 March 2017).
32. von Randow, C.; Manzi, A.O.; Kruijt, B.; de Oliveira, P.J.; Zanchi, F.B.; Silva, R.L.; Hodnett, M.G.; Gash, J.H.C.; Elbers, J.A.; Waterloo, M.J.; et al. Comparative measurements and seasonal variations in energy and carbon exchange over forest and pasture in South West Amazonia. *Theor. Appl. Climatol.* **2004**, *78*, 5–26.
33. Tasumi, M. Progress in Operational Estimation of Regional Evapotranspiration Using Satellite Imagery. Ph.D. Thesis, University of Idaho, Moscow, ID, USA, 2003.
34. Allen, R.; Trezza, R.; Tasumi, M.; Kjaersgaard, J. METRIC Mapping Evapotranspiration at High Resolution using Internalized Calibration. *Appl. Man. Landsat Satell. Imag.* **2014**, *3*, 279.
35. Markham, B.L.; Barker, J.L. Landsat MSS and TM post-calibration dynamic ranges, exoatmospheric reflectances and at-satellitetemperatures. *EOSAT Landsat Tech. Notes* **1986**, *1*, 3–8.
36. ASCE-EWRI. *The ASCE Standardized Reference Evapotranspiration Equation. Report of the ASCE-EWRI Task Committee on Standardization of Reference Evapotranspiration*; ASCE: Reston, VA, USA, 2005; p. 147.
37. Kjaersgaard, J.; Allen, R.; Irmak, A. Improved methods for estimating monthly and growing season ET using metric applied to moderate resolution satellite imagery. *Hydrol. Process.* **2011**, *25*, 4028–4036. [CrossRef]
38. Souza, C.M.; Siqueira, J.V.; Sales, M.H.; Fonseca, A.V.; Ribeiro, J.G.; Numata, I.; Cochrane, M.A.; Barber, C.P.; Roberts, D.A.; Barlow, J. Ten-year Landsat classification of deforestation and forest degradation in the Brazilian Amazon. *Remote Sens.* **2013**, *5*, 5493–5513. [CrossRef]
39. Bastiaanssen, W.G.M. Regionalization of surface flux densities and moisture indicators in composite terrain: A remote sensing approach under clear skies in Mediterranean cimates. Ph.D. Thesis, CIP Data Koninklijke Bibliotheek, Den Haag, The Netherlands, 1995.
40. Allen, R.G.; Pereira, L.S.; Raes, D.; Smith, M. *Crop Evapotranspiration. Guidelines for Computing Crop Water Requirements*; FAO Irrigation and Drainage Paper 56; FAO: Rome, Italy, 1998; p. 300.
41. Perrier, A. Land surface process: Vegetation. In *Land Surface Process in Atmospheric General Circulation Models*; Eagelson, P., Ed.; Cambridge University Press: Cambridge, UK, 1982; pp. 395–448.
42. Twine, T.E.; Kustas, W.P.; Norman, J.M.; Cook, D.R.; Houser, P.R.; Meyers, T.P.; Prueger, J.H.; Starks, P.J.; Wesely, M.L. Correcting Eddy-Covariance Flux Underestimates over a Grassland. *Agric. For. Meteorol.* **2000**, *103*, 279–300. [CrossRef]
43. Wilson, K.; Goldstein, A.; Falge, E.; Aubinet, M.; Baldocchi, D.; Berbigier, P.; Grelle, A. Energy balance closure at FLUXNET sites. *Agric. For. Meteorol.* **2002**, *113*, 223–243. [CrossRef]
44. Almeida, C.A.; Valeriano, D.M.; Escada, M.I.S.; Renno, C.D. Estimativa de área de vegetação secundária na Amazônia Legal Brasileira. *Acta Amazon.* **2010**, *40*, 289–302. [CrossRef]
45. Numata, I.; Roberts, D.A.; Sawada, Y.; Chadwick, O.A.; Schimel, J.P.; Soares, J.V. Regional characterization of pasture changes time and space in Rondonia, Brazil. *Earth Interact.* **2007**, *11*, 1–25. [CrossRef]
46. Nepsted, D.; Lefebvre, P.; Da Silva, U.L.; Tomasella, J.; Schlesinger, P.; Solorzano, L.; Moutinho, P.; Ray, D.; Benito, J.G. Amazon drought and its implications for forest flammability and tree growth: A basin-wide analysis. *Glob. Chang. Biol.* **2004**, *10*, 704–717. [CrossRef]
47. Juarez, R.I.N.; Hodnett, M.G.; Fu, R.; Goulden, M.L.; von Randow, C. Control of dry season evapotranspiration over the Amazonian forest as inferred from observations at a southern Amazon forest site. *J. Clim.* **2007**, *20*, 2827–2839. [CrossRef]
48. Neef, T.; Lucas, R.M.; dos Santos, J.R.; Brondizio, E.S.; Freitas, C.C. Area and age of secondary forests in Brazilian Amazonia 1978–2002: An empirical estimate. *Ecosystems* **2006**, *9*, 609–623. [CrossRef]

49. Aragao, L.E.O.C.; Poulter, B.; Barlow, J.B.; Anderson, L.O.; Malhi, Y.; Saatchi, S.; Phillips, O.L.; Gloor, E. Environmental change and the carbon balance of Amazonian forests. *Biol. Rev.* **2014**, *89*, 913–931. [CrossRef] [PubMed]
50. Brando, P.M.; Balch, J.K.; Nepstad, D.C.; Morton, D.C.; Putz, F.E.; Coe, M.T.; Silverio, D.; Macedo, M.N.; Davidson, E.A.; Nobrega, C.C.; et al. Abrupt increases in Amazonian tree mortality due to drought-fire interactions. *Proc. Natl. Acad. Sci. USA* **2014**, *111*, 6347–6352. [CrossRef] [PubMed]
51. Cochrane, M.A. Fire science for rainforests. *Science* **2003**, *421*, 913–919. [CrossRef] [PubMed]